Carbonaceous aerosols on the south edge of the Tibetan Plateau: concentrations, seasonality and sources

Z. Cong[1, 3, 5], S. Kang[2, 5], K. Kawamura[3], B. Liu[1], X. Wan[1], Z. Wang[1], S. Gao[1], P. Fu[4]

[1]{Institute of Tibetan Plateau Research, CAS, Beijing 100101, China}

[2]{State Key Laboratory of Cryospheric Sciences, CAS, Lanzhou 730000, China}

[3]{Institute of Low Temperature Science, Hokkaido University, Sapporo, 060-0819, Japan}

[4]{LAPC, Institute of Atmospheric Physics, CAS, Beijing 100029, China}

[5]{CAS Center for Excellence in Tibetan Plateau Earth Sciences, Beijing 100101, China}

Correspondence to

S. Kang (shichang.kang@itpcas.ac.cn)

K. Kawamura (kawamura@lowtem.hokudai.ac.jp)

Abstract

To quantitatively evaluate the effect of carbonaceous aerosols on the south edge of the Tibetan Plateau, aerosol samples were collected weekly from August 2009 to July 2010 at Mt. Everest (QOMS, 28.36°N, 86.95°E, 4276 m a.s.l.). The average concentrations of OC, EC and WSOC were 1.43, 0.25 and 0.77 $\mu g\ m^{-3}$, respectively. The concentration levels of OC and EC at QOMS are comparable to those at high elevation sites on the southern slopes of the Himalayas (Langtang and NCO-P), but three to six times lower than those at Manora Peak, India and Godavari, Nepal. Sulfate was the most abundant anion species followed by nitrate, accounting for 25% and 12% of total ionic mass, respectively. Ca^{2+} was the most abundant cation species (annual average of 0.88 $\mu g\ m^{-3}$). The dust loading, represented by Ca^{2+} concentration, was relatively constant throughout the year. OC, EC and other ionic species (NH_4^+, K^+, NO_3^-, and SO_4^{2-}) exhibited a pronounced peak in the pre-monsoon period and a minimum in the monsoon season, being similar to the seasonal trends of aerosol composition reported previously from the southern slope of the Himalayas, such as Langtang and NCO-P. The strong correlation of OC and EC in QOMS aerosols with K^+ and levoglucosan indicates that they were mainly originated from biomass burning. The fire spots observed by MODIS and backward airmass trajectories further demonstrate that in pre-monsoon season, agricultural and forest fires in the northern India and Nepal were most likely sources of carbonaceous aerosol at QOMS. Moreover, the CALIOP observations confirmed that air pollution plumes crossed the Himalayas during this period. The highly coherent variation of daily aerosol optical depth (AOD, 500 nm) between QOMS and NCO-P indicates that both slopes of the Himalayas share a common atmospheric environment regime. In addition to large-scale atmospheric circulation, the unique mountain/valley breeze system can also have an important effect on air pollutant transport.

1 Introduction

The Tibetan Plateau (TP) and the surrounding Hindu Kush-Himalayan mountains are known as the "Third Pole" of the Earth (Qiu, 2008), due to its immense area and high elevation (Yao et al., 2012). Because of the contrast of thermal heating between continent and ocean, the TP plays a fundamental role in the formation of the Asian monsoon system and Northern Hemispheric climatology (Wu and Zhang, 1998). The TP and Himalayas, with more than 100,000 km^2 of glaciers, contain the largest ice mass outside the Polar region (Xu et al., 2009;Yao et al., 2012). Over the past decades, climate change impacts have been revealed due to marked air temperature rising and dramatic glacier shrinkage across this area (Kang et al., 2010).

Due to sparse population and minimal industrial activities, the TP is considered one of the most pristine terrestrial regions, alongside the Arctic and Antarctic. However, growing evidence has demonstrated that widespread atmospheric brown clouds (ABCs) over South Asia may affect this region (Bonasoni et al., 2010;Kaspari et al., 2011;Lu et al., 2012;Xia et al., 2011;Wang et al., 2010). Research has attempted to reveal a link between climate change over the TP (e.g. air temperature rising, glacier melting) and the distribution of anthropogenic pollutants (mainly absorbing carbonaceous materials) (Qian et al., 2015;Wang et al., 2014b). Ramanathan and Carmichael (2008) reported that in the high Himalayan region, solar heating caused by black carbon (BC) could be approximately equivalent to the warming by CO_2 in terms of the melting of snowpack and glaciers.

Could we quantitatively differentiate the various factors that contribute to glacier melting, including aerosols, greenhouse gas, and BC deposition on the snow surface? Clearly, to answer this question and reduce the uncertainties, adequate knowledge of the aerosol properties is urgently needed. Some scientists have used different models to reveal the importance of carbonaceous aerosol in this region (Menon et al., 2010;Qian et al., 2011;Yasunari et al., 2010). So far, most works on aerosol composition have been carried out on the south slope of the Himalayas, such as Langtang, Nepal (Carrico et al., 2003), Godavari (Stone et al., 2010), Nepal Climate

Observatory-Pyramid (NCO-P) (Decesari et al., 2010) and Manora Peak, India (Ram et al., 2010). Long-term aerosol chemistry measurements from the TP are extremely scarce mainly due to its remoteness and challenging weather conditions, with measurements limited to Lulang (Zhao et al., 2013), Waliguan (Ma et al., 2003), Nam Co (Ming et al., 2010) and Qinghai Lake (Li et al., 2013). As we know, no systematic data on carbonaceous aerosols from the south edge of the TP (i.e. the north slope of Himalayas) has been reported. From the spatial distribution of aerosols observed by satellites (e.g. MODIS, Fig. S1), there was a clear difference between South Asia and Tibetan Plateau. Therefore, as the boundary area this region merits special attention.

In this paper, we present results from one-year measurements of organic carbon (OC), elemental carbon (EC), water-soluble organic carbon (WSOC) and major ions in the aerosols at Mt. Everest, the south edge of the TP. Our aim is to provide baseline levels of aerosols for this region, reduce the assessment uncertainties of aerosol radiative forcing and provide more information on their transport mechanism.

2   Methodology

2.1 Description of research site

In 2005, Qomolangma (Mt. Everest) Station for Atmospheric and Environmental Observation and Research (briefly QOMS, 28.36°N, 86.95°E, 4276 m a.s.l.) (Fig. 1) was established to begin continuous monitoring of the environment (Ma et al., 2011). A solar electricity system generates the power to maintain the instrumentation. According to the observations achieved so far, the Mt. Everest region (QOMS) is a typical representative of the middle Himalayas in terms of climate, air circulation systems and environmental characteristics (Chen et al., 2012;Li et al., 2012;Ma et al., 2011). Sandy soil with sparse grass and small rocks cover the land surface around the QOMS. Due to its harsh environment, QOMS is relatively isolated from industrial zone and cities, with a very limited local population (Ma et al., 2011).

2.2 Aerosol sampling

From August 2009 to July 2010, total suspended aerosol particle (TSP) samples were collected weekly at QOMS using medium-volume samplers (KC-120H, Laoshan Co.). During the sampling, the flow rate was automatically adjusted to 100 L min^{-1} at standard condition. The sampling duration of each sample was 24 hours. Aerosols were collected using 90-mm diameter quartz filters (QM/A, Whatman, UK), which were pre-combusted at 450 °C for 6 hours. Field blanks were collected every month by placing filters into the filter holder for a few minutes with no air flowing. After sampling, the filters were wrapped with aluminum foil and frozen until analysis. Eventually, fifty samples were successfully obtained.

2.3 OC and EC analysis

The quartz filters were analyzed for OC and EC using a carbon analyzer (DRI model 2001). Briefly, a filter aliquot (0.5 cm^2) was analyzed for eight carbon fractions following the IMPROVE-A thermal/optical reflectance (TOR) protocol (Cao et al., 2007;Chow et al., 2007). Four OC fractions (OC1, OC2, OC3 and OC4) were determined at 140, 280, 480 and 580 °C in pure He atmosphere, which was subsequently switched to 2% O_2/98% He atmosphere to determine EC1, EC2 and EC3 at 580, 740 and 840 °C, respectively. The residence time of each heating step was defined by the flattening of the carbon signal. The pyrolyzed carbon fraction (OPC) is determined when reflected laser light returns to its initial value after oxygen is introduced. In general, OC is defined as OC1 + OC2 + OC3 + OC4 + OPC and EC is defined as EC1 + EC2 + EC3 - OPC. The detection limit for the carbon analyzer was 0.05 μgC cm^{-2} for OC and 0.05 μg C cm^{-2} for EC.

2.4 Water-soluble ions and WSOC

An aliquot of filter (2.54 cm^2) was extracted with 10 ml ultrapure water with sonication for 30 minutes. The extracted solutions were filtrated with syringe-driven filters (Millex-GV PVDF, 0.22 μm; Millipore, Ireland) to remove the quartz fiber debris and other insoluble impurities. Then the water-soluble ionic species (Cl^-, SO_4^{2-},

132 NO_3^-, Ca^{2+}, Na^+, K^+, Mg^{2+} and NH_4^+) were analyzed using an ion chromatograph (761

133 Compact IC, Metrohm). Anions were measured with a suppressor on a Shodex SI-90

134 4E column using an eluent mixture of 1.8 mM Na_2CO_3, 1.7 mM $NaHCO_3$ and 40 mM

135 H_2SO_4 at a flow rate of 1.2 mL min^{-1}. Cations were determined on a Metrohm C2-150

136 column with tartaric acid (4 mM) and dipicolinic acid (1 mM) as an eluent. The

137 overall uncertainty in determining ionic species is less than 4% (Miyazaki et al.,

138 2010). The detection limit for all cations and anions was 0.01 μg m^{-3}, which was

139 calculated according to the air volume of actual samples.

140 To quantify WSOC, a portion of filter (19.1 cm^2) was extracted and filtrated using the

141 same procedure for major ions described above. Then the extract was injected into a

142 total carbon analyzer (TOC-V, Shimadzu). The method detection limit (MDL) used

143 was 4 μg L^{-1} with a precision of ±5%. All the concentrations of carbonaceous and

144 ionic components in this study are field-blank corrected. It should be noted that there

145 are possible sampling artifacts by the adsorption/evaporation of gaseous organic

146 materials on/from the quartz membrane. However, no quantitative information on

147 such positive/negative artifact is available in this study, therefore, no correction was

148 made for the data of carbonaceous components.

149 **2.5 Determination of levoglucosan**

150 Levoglucosan was determined by GC/MS after the extraction of the samples with a

151 methanol/methylene chloride mixture followed by BSTFA derivatization. Details of

152 the analytical procedure is presented elsewhere (Fu et al., 2008).

153 **2.6 Meteorology and backward air mass trajectories**

154 At the QOMS station, various meteorological parameters (Fig. 2) were recorded by a

155 40 m atmospheric boundary layer tower that measures wind speeds, wind direction

156 (014A-L, Met One), relative humidity, air temperature, air pressure (HMP45C,

157 Vaisala) and rain intensity (TE525MM-L, Young) (Chen et al., 2012;Li et al., 2012).

158 Monthly mean air temperature reaches a maximum of 12.3°C in July, with a

159 minimum in January of -3.2°C. Humidity is highest in August while lowest in

160   December. Precipitation was unevenly distributed throughout the year, with more

161   than 90% of annual precipitation occurring from June to September. According to the

162   meteorological parameters at QOMS (Fig. 2), the climatology is roughly divided into

163   four seasons, i.e. pre-monsoon, monsoon, post-monsoon and winter (The definition of

164   different seasons was shown in Table S1). These seasons are generally in agreement

165   with the seasonal definition made in a previous study in this region (Bonasoni et al.,

166   2010). In general, this region is controlled by Indian Monsoon system in summer

167   (June-August), characterized by relatively high temperature and humid weather with

168   prevailing southerly winds. While in the remaining period, westerlies dominate the

169   large-scale atmospheric circulation patterns with limited precipitation.

170   To reveal the transport pathway of air masses that arrive at QOMS, seven-day

171   backward trajectories were computed using the HYSPLIT model (Draxler and Rolph,

172   2012) and GDAS (Global Data Assimilation System) data for each sampling day.

173   Given the typical height of the planetary boundary layer (PBL) in this region (Chen et

174   al., 2012), the arrival height of air mass in these modeling was set to 500 m above

175   ground level.

176

177   3   Results and discussion

178   3.1 Characteristics and temporal variations of OC and EC

179   The statistical summaries of carbonaceous components in the aerosols from QOMS

180   are presented in Table 1. The average concentrations of OC and EC in the aerosols

181   from QOMS were 1.43 ± 1.16 and 0.25 ± 0.22 μg m^{-3}, respectively. The concentration

182   levels of OC and EC at QOMS are about three times higher than those of Muztagh

183   Ata, northwest TP (Cao et al., 2009), while they are comparable to those reported

184   from the Central and Northeastern TP (Li et al., 2013;Ming et al., 2010) (Table 2). In

185   contrast, OC and EC concentrations from the southeastern TP (Tengchong and Lulang)

186   are significantly higher than those at QOMS, possibly due to the higher contribution

187   of biomass burning (Engling et al., 2011;Zhao et al., 2013). When compared with

188 sites on the south slopes of the Himalayas, QOMS data present the same order of OC

189 and EC with NCO-P (Decesari et al., 2010) and Langtang (Carrico et al., 2003), but

190 three to six-fold lower than Manora Peak, India (Ram et al., 2010) and Godavari,

191 Nepal (Stone et al., 2010). The latter two sites are at lower altitudes and are closer to

192 the populated areas of South Asia, heavily influenced by anthropogenic emission.

193 Generally, the high altitude sites on both sides of the Himalayas (i.e. Langtang,

194 NCO-P and QOMS) exhibit similar OC and EC abundance, which could be

195 considered as a regional baseline level to be used in the regional climate model as

196 input parameters.

197 In a previous study, Ming et al. (2008) estimated atmospheric EC concentration in the

198 region based on the analysis of an ice core from the East Rongbuk Glacier, Mt.

199 Everest. Apparently, there is a big discrepancy between our EC data (annual average

200 of 0.25 ± 0.22 μg m^{-3}) and the EC data estimated by ice cores (average: 0.077 ± 0.045

201 μg m^{-3} during 1951–2001). One potential reason is that several parameters (e.g.

202 scavenging ratio of EC) need to be assumed to convert the EC in the ice core to

203 atmospheric concentration, which may introduce some uncertainty. Moreover,

204 dramatically increasing trends of EC in the Himalayas and the TP ice cores have been

205 reported (Cong et al., 2013;Kaspari et al., 2011), i.e. a two and a half to three fold rise

206 in recent decades compared to background conditions. Therefore, our EC data for

207 2009–2010, which is higher than the average EC concentration for 1951–2001, is

208 reasonable.

209 The OC/EC ratios at QOMS range from 1.91 to 43.8, with average of 6.69. Such high

210 ratios are commonly found in different areas of the TP (Table 2). There are two

211 potential reasons for those high OC/EC ratios. One reason may be a strong solar

212 radiation (exceeding 7500 MJ m^{-2}) over the TP, because substantial secondary organic

213 carbon (SOC) could be formed through photochemical reaction (Wan et al., 2015).

214 The other potential reason is the influence of biomass burning. Usually, the aerosols

215 emitted from biomass burning have higher OC/EC ratio. For example, Watson et al.

216 (2001) have reported an OC/EC ratio of 14.5 for forest fires. Considering the specific

condition of this study (QOMS), the second reason is more likely, i. e. the strong influence of biomass-burning emissions. The higher abundance of OC than EC on the TP emphasizes that OC should not be ignored in the quantification of total radiative forcing of aerosol by climate models (Kopacz et al., 2011). Although some organic carbon has light-absorbing capability (i.e. brown carbon), the net effect of organic carbon on climate is negative (cooling) (Stocker et al., 2013), which may attenuate the positive radiative forcing caused by EC.

The temporal variations of the aerosol OC, EC and WSOC are illustrated in Fig. 3. Clearly, the OC, EC and WSOC share a significant seasonal pattern，i.e. a maximum in the pre-monsoon period and a minimum in the monsoon season. Higher abundance of OC and EC implies that the contributions from anthropogenic activities are larger in pre-monsoon than other seasons. Similar seasonal trends of aerosol composition were also reported previously on the south slopes of the Himalayas, such as Langtang (Carrico et al., 2003) and NCO-P (Decesari et al., 2010). This phenomenon indicates that these regions (Mt. Everest), both slopes of the Himalayas, have a common atmospheric environmental regime, although the high altitude of the Himalayas was once considered a good barrier for the spreading of atmospheric pollutants in South Asia. This point will be further discussed in Section 3.5.

3.2 Relationship between OC and EC

Examining the relationship between OC and EC can provide meaningful insights into the origin and possible reaction process during the transport of carbonaceous aerosols (Turpin and Huntzicker, 1995). At QOMS, a strong correlation ($R^2 = 0.81$) was observed between OC and EC during the pre-monsoon season (Fig. 4a), indicating common emission sources and transport processes. The correlation coefficients between OC and EC in the other three seasons were lower than that of the pre-monsoon season (Fig. 4b, c, d), with the lowest correlation observed in the summer monsoon season ($R^2 = 0.08$), suggesting that there are other influences. In addition to the common emission sources (e.g. fossil fuel and biomass burning), OC could also be produced by biogenic sources and the formation of secondary OC

246 (SOC). The relative importance of different sources and/or formation process merits a

247 further study.

248 SOC has often been calculated from the primary OC/EC ratio (EC-tracer method)

249 ($OC_{pri} = EC*(OC/EC)_{min}$, $OC_{sec} = OC_{tot} - OC_{pri}$), which is assumed to be relatively

250 constant for a given site (Turpin and Huntzicker, 1995). The lowest OC/EC ratio in

251 the aerosol was suggested for use as the primary source to calculate the SOC

252 abundance (Castro et al., 1999), when the secondary production of OC is expected to

253 be minimal. However, for the samples from QOMS, we found that calculating SOC

254 formation using this method was not reliable. The minimum OC/EC ratios differ

255 greatly among various seasons (3.40, 3.78, 1.91 and 2.67 for pre-monsoon, monsoon,

256 post-monsoon and winter, respectively). Even for each season (11–13 samples for

257 each seasons), the lowest three values of OC/EC ratios also varied substantially.

258 Therefore, the SOC formation estimated by the conventional EC-tracer method is not

259 presented here.

260 **3.3 Water-Soluble Organic Carbon (WSOC)**

261 The WSOC in aerosols, a major proportion of total organic carbon, could affect the

262 hygroscopic property of the particles and their ability to act as cloud condensation

263 nuclei (CCN) (Psichoudaki and Pandis, 2013). The abundance of WSOC relative to

264 OC could be employed as an indictor to decipher whether organic aerosol is primary

265 or secondary, because SOC usually tends to be more water-soluble than primary

266 organic matter (Psichoudaki and Pandis, 2013). The concentration of WSOC at

267 QOMS varied from 0.07 to 3.22 µg m^{-3}, with an average of 0.77 µg m^{-3} (Table 1). The

268 average WSOC/OC ratios at QOMS were 0.47, 0.59, 0.62 and 0.57 for pre-monsoon,

269 monsoon, post-monsoon and winter, respectively. The lowest WSOC/OC in

270 pre-monsoon indicated the dominant contribution from primary emission sources with

271 poor aging and less SOA formation. Furthermore, in the pre-monsoon season, the

272 WSOC concentration exhibited a significant positive correlation with OC (y =

273 0.54x-0.12, $R^2 = 0.94$), which could be ascribed to the influence of biomass

274 combustion. Previous studies have revealed that organic matters emitted from

275   biomass burning were substantially composed of water-soluble polar organic

276   compounds, including dicarboxylic acids, sugars, aromatic acids, etc. (Claeys et al.,

277   2010;Fu et al., 2012;Kundu et al., 2010). No evident correlation was found between

278   WSOC and OC in other seasons when OC concentrations were low (Fig. 5).

279   **3.4 Water-Soluble Ionic Species (WSIS)**

280   Sulfate was the most abundant anion species followed by nitrate, accounting for 25%

281   and 12% of total ionic mass, respectively (Table 1). Ca^{2+} was the most abundant

282   cation species with annual average of 0.88 μg m^{-3}. Cl$^-$ and Na$^+$ only consisted of a

283   very minor portion of total ions, indicating that at QOMS the influence of sea salt is

284   negligible. Water-soluble Ca^{2+} is a typical tracer of crustal material (dust) (Ram et al.,

285   2010). At QOMS, the time-series of Ca^{2+} was somewhat uniform throughout the years

286   (Fig. 6), implying that the mineral dust loading at QOMS is relatively constant. This

287   pattern was obviously in contrast to other ionic species (NH_4^+, K^+, NO_3^-, and SO_4^{2-}).

288   The temporal variation patterns of Ca^{2+} and SO_4^{2-} are different (Fig. 6), and thus the

289   correlation is not strong ($R^2 = 0.27$), which excludes the possibility that they

290   predominantly co-occurred in some minerals (e.g. gypsum).

291   Soluble potassium (K^+) is a good tracer of biomass burning (Andreae and Merlet,

292   2001;Cachier et al., 1995). In our study, the K^+ concentrations were below detection

293   limit in most samples, but K^+ concentrations did show peaks in pre-monsoon season

294   (Fig. 6). Furthermore, K^+ and EC demonstrated a good relationship ($R^2 = 0.66$, n = 9)

295   during that period, indicating that they were both derived from biomass burning (Fig.

296   7c). A significant correlation between NO_3^- and SO_4^{2-} was not surprising (Fig. 7a),

297   because they generally form from the oxidation of NOx and SO_2, which are closely

298   related to fossil fuel combustion. In the pre-monsoon season with a high abundance of

299   NH_4^+ (Fig. 6), NH_4^+ and NO_3^- exhibited a good correlation ($R^2 = 0.80$, n = 9),

300   implying that they are present as NH_4NO_3 in the aerosol particles.

301   The seasonal variation of biomass burning (K^+) coincided with that of ions associated

302   with the fossil fuel combustion (NH_4^+, NO_3^-, and SO_4^{2-}), suggesting that in the

303   pre-monsoon season, QOMS might have received mixed anthropogenic pollution. But

304 another explanation is more plausible. According to earlier observation by

305 transmission electron microscopy (Li et al., 2003), large amounts of K_2SO_4 and KNO_3

306 were present in aged smoke aerosols from biomass burning. Andreae et al. (1988)

307 pointed out that haze aerosol from biomass burning is comprised of abundant NH_4^+,

308 K^+, NO_3^- and SO_4^{2-}. Similarly, NH_4^+, K^+, NO_3^- and SO_4^{2-} are also reported as major

309 water-soluble inorganic ions in aerosols from biomass burning on the southeastern

310 Tibetan Plateau (Engling et al., 2011). In addition to K^+, levoglucosan is also used as

311 a specific marker for biomass burning, which is formed by the pyrolysis of cellulose

312 but not formed by fossil fuel combustions (Simoneit et al., 1999). In the pre-monsoon

313 season, EC, OC and K^+ show good correlations with levoglucosan (Fig. 8), which

314 further indicate that carbonaceous components in QOMS aerosols were

315 predominantly from biomass burning.

316 **3.5 Transport mechanism of aerosols**

317 Seven-day backward air mass trajectories corresponding to each sampling date were

318 calculated using the Hysplit model (Draxler and Rolph, 2012). Seven days were

319 chosen because of the typical residence time of carbonaceous aerosols in atmosphere.

320 The trajectories were generally consistent with other descriptions of air circulation

321 patterns in previous studies (Cong et al., 2009), which correspond to the South Asian

322 monsoon regime (Fig. 9). In the summer monsoon season, air masses are derived

323 from Bangladesh and northeast India, and bring moisture that originates in the Bay of

324 Bengal. In the non-monsoon season, strong westerlies pass through western Nepal,

325 northwest India, and Pakistan (i.e. Southern Himalayas). Although the transport

326 pathways of air masses arriving at QOMS during pre-monsoon, post-monsoon and

327 winter are similar (Fig. 9), a distinctly higher carbonaceous aerosol level was found

328 only in the pre-monsoon season (Fig. 3), which emphasizes the importance of source

329 strength changes.

330 According to the previous ABC research (Ramanathan et al., 2005) and the emission

331 inventory (Wang et al., 2014a), a high loading of atmospheric pollutants exists over

332 the southern slopes of the Himalayas, which was pronounced in the pre-monsoon

season. We further checked the biomass burning emission from different seasons using the active fire product from MODIS (MODerate-resolution Imaging Spectroradiometer, both Terra and Aqua dataset), which was provided by Fire Information for Resource Management System (FIRMS, https://earthdata.nasa.gov/firms). Figure 10 clearly shows that the active fire counts (representing the agricultural burning and forest fires) peaked in pre-monsoon (April). This finding is in agreement with the vegetation fire study on the southern slopes of the Himalayas by Vadrevu et al. (2012). In general, the seasonal pattern of carbonaceous components (OC, EC and WSOC), their strong correlation with K^+ and levoglucosan, together with the air mass trajectories and active fire spots distribution, all suggest that the higher loadings of carbonaceous aerosols in the pre-monsoon season at QOMS were most likely affected by the biomass burning (agricultural and forest fires) in northern India and Nepal.

In addition to the large-scale atmospheric circulation, the local orographic effect on air pollutant transport should also be taken into account (Hindman and Upadhyay, 2002). In mountainous areas, because of the temperature difference between mountaintop and lowland, a diurnal valley wind system occurs that blows upward during the day and reverses into downward during the night. As shown by Bonasoni et al. (2010), the wind regime at NCO-P (southern slope of the Himalayas) was characterized by an evident daily circle of mountain/valley breeze. During the daytime, the valley winds (southerly) were predominant with maximum wind speed in the afternoon. Therefore, the daytime up-valley breeze delivered the air pollutants from the foothills (South Asia ABC) to higher altitudes (>5000 m a.s.l.). Aerosol mass concentration, BC and ozone at NCO-P exhibit strong diurnal cycles, with minima during the night and maxima during the afternoon especially in the pre-monsoon season (Decesari et al., 2010;Marinoni et al., 2010). However, distinct mountain-valley breeze circulation was observed on the northern slopes of the Himalayas (QOMS). A dominating down-valley wind occurs on the north side of Mt. Everest in the daytime, especially in the afternoon. Further, the driving force of the

362 vast snow cover at high altitude could form a "glacier wind", and the up-valley air

363 flow produced by intense ground surface heating is overcome by down-valley air flow

364 "glacier wind" and "mountain wind" (Chen et al., 2012;Zou et al., 2008). Therefore,

365 daytime intense valley wind circulation could make the valleys efficient channels for

366 the transport of air pollutants crossing over the Himalayas (Fig. S2), i.e., from the low

367 altitude of South Asia to the Tibetan Plateau.

368 Because both QOMS and NCO-P have sun-photometers and participated in the

369 AERONET project, the same instrument (Cimel 318), the same data processing

370 method and simultaneous observation between QOMS and NCO-P make it possible to

371 compare AOD data directly between the two slopes of Himalayas (Xu et al.,

372 2014;Gobbi et al., 2010). As shown in Figure 11, the daily AOD (500 nm) of QOMS

373 and NCO-P varied in highly similar pattern (The correlation significant at $p<0.001$),

374 which suggesting that the observation at QOMS can also capture the pollution signals

375 as NCO-P. Recently, Lüthi et al. (2014) investigated the transport mechanisms of

376 pollutants across Himalayas using a high-resolution model. They found some

377 trajectories with low altitudes originate from the TP, and then flow down through

378 valleys to the foothills of Himalayas during nighttime where they can mix with air

379 pollutants, and are then blown onto the TP again during daytime. For the vertical

380 distribution of aerosols, two examples of such transport episode revealed by CALIOP

381 satellite now were provided in the Supplementary Information (Fig. S3), which

382 clearly showed the pollution plumes from South Asia could transport across

383 Himalayas during the pre-monsoon season.

384 We roughly estimated the timescale for air masses transported from the southern slope

385 of Mt. Everest (NCO-P) to QOMS. The straight distance between the two sites is

386 about 40 km, and along the valley the real distance is about 50 km if we consider the

387 terrain effect (Fig. 1). The average wind speed in pre-monsoon season is 7.86 m/s

388 (Table S1). This means that the air mass could travel from the southern slope of Mt.

389 Everest and reach QOMS in less than two hours, even at the average wind speed.

390 These results demonstrate that at QOMS we can capture the air pollution signal from

391   the southern Himalayas. This air mass transport of pollutants caused by mountain

392   terrain along the valley was also supported by WRF modeling, i.e. at the upper valley

393   there is a pronounced southerly flow onto the Tibetan Plateau (Bonasoni et al., 2010).

394   In this study, a similar seasonal trend of aerosol composition was revealed between

395   the southern and northern slopes of the Himalayas. The most probable explanation is

396   that the local mountain/valley breeze circulation (south-to north air flow) acts as the

397   connection for the air pollutants crossing the Himalayas.

398

399   **4   Summary and conclusions**

400   A comprehensive knowledge of aerosol chemistry is crucial for assessing

401   anthropogenic influences and evaluating the effect of radiative forcing. This research

402   presents the first dataset of carbonaceous aerosols for the south edge of the Tibetan

403   Plateau. The average concentrations of OC and EC in the aerosols at QOMS were

404   1.43 and 0.25 $\mu g\ m^{-3}$, with a standard deviation of 1.16 and 0.22 $\mu g\ m^{-3}$, respectively.

405   The high altitude sites from both sides of the Himalayas (i.e. Langtang, NCO-P and

406   QOMS) exhibit similar OC and EC abundances, which could be considered as a

407   regional baseline level to be used as input parameters in the regional climate model.

408   The most striking finding in this study is that carbonaceous components (OC, EC and

409   WSOC) and several ionic species (NH_4^+, K^+, NO_3^- and SO_4^{2-}) exhibit a clear seasonal

410   pattern with concentration maxima in the pre-monsoon season (March, April and

411   May). A strong correlation ($R^2 = 0.81$) was observed between OC and EC during the

412   pre-monsoon season, indicating their common emission sources and transport process.

413   The EC and OC show good correlations with biomass burning tracers (K^+ and

414   levoglucosan), which further suggests that carbonaceous components in QOMS

415   aerosols mainly originate from biomass burning. Based on the active fire spots

416   observed by MODIS and backward trajectories, we found that in pre-monsoon,

417   agricultural and forest fires in northern India and Nepal are the most likely sources of

418   carbonaceous aerosol at QOMS. In addition to large-scale atmospheric circulation

419   (South Asia monsoon system and westerlies), local mountain wind systems can also

420   play an important role. The south-to-north airflow along mountain valleys in the

421   Himalayas could closely connect the atmospheric environment between the two sides

422   of the Himalayas. A higher time resolution research (diurnal) is imperative in the

423   future to deepen our understanding of such important processes.

424

Acknowledgements

436

References

Andreae, M. O., Browell, E. V., Garstang, M., Gregory, G., Harriss, R., Hill, G., Jacob, D., Pereira, M., Sachse, G., and Setzer, A.: Biomass‐burning emissions and associated haze layers over Amazonia, J. Geophys. Res. -Atmos., 93, 1509-1527, 1988.

Andreae, M. O., and Merlet, P.: Emission of trace gases and aerosols from biomass burning, Global biogeochem. cy., 15, 955-966, 2001.

Bonasoni, P., Laj, P., Marinoni, A., Sprenger, M., Angelini, F., Arduini, J., Bonafè, U., Calzolari, F., Colombo, T., Decesari, S., Di Biagio, C., di Sarra, A. G., Evangelisti, F., Duchi, R., Facchini, M. C., Fuzzi, S., Gobbi, G. P., Maione, M., Panday, A., Roccato, F., Sellegri, K., Venzac, H., Verza, G. P., Villani, P., Vuillermoz, E., and Cristofanelli, P.: Atmospheric Brown Clouds in the Himalayas: first two years of continuous observations at the Nepal Climate Observatory-Pyramid (5079 m), Atmos. Chem. Phys., 10, 7515-7531, 10.5194/acp-10-7515-2010, 2010.

Cachier, H., Liousse, C., Buat-Menard, P., and Gaudichet, A.: Particulate content of savanna fire emissions, J. Atmos. Chem., 22, 123-148, 1995.

Cao, J., Lee, S., Chow, J., Watson, J., Ho, K., Zhang, R., Jin, Z., Shen, Z., Chen, G., and Kang, Y.: Spatial and seasonal distributions of carbonaceous aerosols over China, J. Geophys. Res. -Atmos., 112, D22S11, doi:10.1029/2006JD008205, 2007.

Cao, J., Xu, B., He, J., Liu, X., Han, Y., Wang, G., and Zhu, C.: Concentrations, seasonal variations, and transport of carbonaceous aerosols at a remote Mountainous region in western China, Atmos. Environ., 43, 4444-4452, 2009.

Carrico, C. M., Bergin, M. H., Shrestha, A. B., Dibb, J. E., Gomes, L., and Harris, J. M.: The importance of carbon and mineral dust to seasonal aerosol properties in the Nepal Himalaya, Atmos. Environ., 37, 2811-2824, 2003.

Castro, L., Pio, C., Harrison, R. M., and Smith, D.: Carbonaceous aerosol in urban and rural European atmospheres: estimation of secondary organic carbon concentrations, Atmos. Environ., 33, 2771-2781, 1999.

Chen, X., Su, Z., Ma, Y., and Sun, F.: Analysis of Land-Atmosphere Interactions over the North Region of Mt. Qomolangma (Mt. Everest), Arct. Antarct. Alp. Res., 44, 412-422, 2012.

Chow, J. C., Watson, J. G., Chen, L. W. A., Chang, M. C. O., Robinson, N. F., Trimble, D., and Kohl, S.: The IMPROVE-A temperature protocol for thermal/optical carbon analysis: maintaining consistency with a long-term database, J. Air Waste Manage., 57, 1014-1023, 2007.

Claeys, M., Kourtchev, I., Pashynska, V., Vas, G., Vermeylen, R., Wang, W., Cafmeyer, J., Chi, X., Artaxo, P., and Andreae, M.: Polar organic marker compounds in atmospheric aerosols during the LBA-SMOCC 2002 biomass burning experiment in Rondônia, Brazil: sources and source processes, time series, diel variations and size distributions, Atmos. Chem. Phys., 10, 9319-9331, 2010.

Cong, Z., Kang, S., and Qin, D.: Seasonal features of aerosol particles recorded in snow from Mt. Qomolangma (Everest) and their environmental implications, J. Environ. Sci., 21, 914-919, 10.1016/s1001-0742(08)62361-x, 2009.

Cong, Z., Kang, S., Gao, S., Zhang, Y., Li, Q., and Kawamura, K.: Historical Trends of Atmospheric Black Carbon on Tibetan Plateau As Reconstructed from a 150-Year Lake Sediment Record, Environ. Sci. Technol., 47, 2579-2586, 2013.

481 Decesari, S., Facchini, M. C., Carbone, C., Giulianelli, L., Rinaldi, M., Finessi, E., Fuzzi, S., Marinoni, A.,
482   Cristofanelli, P., Duchi, R., Bonasoni, P., Vuillermoz, E., Cozic, J., Jaffrezo, J. L., and Laj, P.:
483   Chemical composition of PM10 and PM1 at the high-altitude Himalayan station Nepal
484   Climate Observatory-Pyramid (NCO-P) (5079 m a.s.l.), Atmos. Chem. Phys., 10,
485   4583-4596, 2010.
486 Draxler, R. R., and Rolph, G. D.: HYSPLIT (HYbrid Single-Particle Lagrangian Integrated Trajectory)
487   Model access via NOAA ARL READY Website, http://ready.arl.noaa.gov/HYSPLIT.php
488   NOAA Air Resources Laboratory, Silver Spring, MD., (last access: Jan. 7th, 2015), 2012.
489 Engling, G., Zhang, Y.-N., Chan, C.-Y., Sang, X.-F., Lin, M., Ho, K.-F., Li, Y.-S., Lin, C.-Y., and Lee, J. J.:
490   Characterization and sources of aerosol particles over the southeastern Tibetan Plateau
491   during the Southeast Asia biomass-burning season, Tellus B, 63, 117-128, 2011.
492 Fu, P., Kawamura, K., Okuzawa, K., Aggarwal, S. G., Wang, G., Kanaya, Y., and Wang, Z.: Organic
493   molecular compositions and temporal variations of summertime mountain aerosols over
494   Mt. Tai, North China Plain, J. Geophys. Res. -Atmos., 113, DOI: 10.1029/2008JD009900,
495   2008.
496 Fu, P., Kawamura, K., Chen, J., Li, J., Sun, Y., Liu, Y., Tachibana, E., Aggarwal, S., Okuzawa, K., and
497   Tanimoto, H.: Diurnal variations of organic molecular tracers and stable carbon isotopic
498   composition in atmospheric aerosols over Mt. Tai in the North China Plain: an influence
499   of biomass burning, Atmos. Chem. Phys., 12, 8359-8375, 2012.
500 Gobbi, G., Angelini, F., Bonasoni, P., Verza, G., Marinoni, A., and Barnaba, F.: Sunphotometry of the
501   2006–2007 aerosol optical/radiative properties at the Himalayan Nepal Climate
502   Observatory-Pyramid (5079 m asl), Atmos. Chem. Phys., 10, 11209-11221, 2010.
503 Hindman, E. E., and Upadhyay, B. P.: Air pollution transport in the Himalayas of Nepal and Tibet
504   during the 1995–1996 dry season, Atmos. Environ., 36, 727-739, 2002.
505 Kang, S., Xu, Y., You, Q., Flügel, W. A., Pepin, N., and Yao, T.: Review of climate and cryospheric
506   change in the Tibetan Plateau, Environ. Res. Lett., 5, 015101 doi:10.1088/1748-
507   9326/5/1/015101, 2010.
508 Kaspari, S., Schwikowski, M., Gysel, M., Flanner, M., Kang, S., Hou, S., and Mayewski, P.: Recent
509   increase in black carbon concentrations from a Mt. Everest ice core spanning 1860-2000
510   AD, Geophys. Res. Lett, 38, L04703, doi:04710.01029/02010GL046096, 2011.
511 Kopacz, M., Mauzerall, D. L., Wang, J., Leibensperger, E. M., Henze, D. K., and Singh, K.: Origin and
512   radiative forcing of black carbon transported to the Himalayas and Tibetan Plateau,
513   Atmos. Chem. Phys., 11, 2837-2852, 2011.
514 Kundu, S., Kawamura, K., Andreae, T. W., Hoffer, A., and Andreae, M. O.: Diurnal variation in the
515   water-soluble inorganic ions, organic carbon and isotopic compositions of total carbon
516   and nitrogen in biomass burning aerosols from the LBA-SMOCC campaign in Rondônia,
517   Brazil, J. Aerosol Sci., 41, 118-133, 2010.
518 Li, J., Pósfai, M., Hobbs, P. V., and Buseck, P. R.: Individual aerosol particles from biomass burning
519   in southern Africa: 2, Compositions and aging of inorganic particles, J. Geophys. Res.
520   -Atmos., 108, 8484, 10.1029/2002JD002310, 2003.
521 Li, J. J., Wang, G. H., Wang, X. M., Cao, J. J., Sun, T., Cheng, C. L., Meng, J. J., Hu, T. F., and Liu, S. X.:
522   Abundance, composition and source of atmospheric PM 2.5 at a remote site in the
523   Tibetan Plateau, China, Tellus B, 65, 2013.
524 Li, M., Ma, Y., and Zhong, L.: The turbulence characteristics of atmospheric surface layer on the

north slope of Mt. Everest region in the spring of 2005, J. Meteorol. Soc. Jpn., 90, 185-193, 2012.

Lu, Z., Streets, D. G., Zhang, Q., and Wang, S.: A novel back-trajectory analysis of the origin of black carbon transported to the Himalayas and Tibetan Plateau during 1996-2010, Geophys. Res. Lett., 39, L01809, doi:01810.01029/02011GL049903, 2012.

Lüthi, Z. L., Škerlak, B., Kim, S. W., Lauer, A., Mues, A., Rupakheti, M., and Kang, S.: Atmospheric brown clouds reach the Tibetan Plateau by crossing the Himalayas, Atmos. Chem. Phys. Discuss., 14, 28105-28146, 10.5194/acpd-14-28105-2014, 2014.

Ma, J., Tang, J., Li, S. M., and Jacobson, M. Z.: Size distributions of ionic aerosols measured at Waliguan Observatory: Implication for nitrate gas‐to‐particle transfer processes in the free troposphere, J. Geophys. Res. -Atmos., 108, 2003.

Ma, Y., Wang, Y., Zhong, L., Wu, R., Wang, S., and Li, M.: The Characteristics of Atmospheric Turbulence and Radiation Energy Transfer and the Structure of Atmospheric Boundary Layer over the Northern Slope Area of Himalaya, J. Meteorol. Soc. Jpn., 89A, 345-353, 2011.

Marinoni, A., Cristofanelli, P., Laj, P., Duchi, R., Calzolari, F., Decesari, S., Sellegri, K., Vuillermoz, E., Verza, G., and Villani, P.: Aerosol mass and black carbon concentrations, a two year record at NCO-P (5079 m, Southern Himalayas), Atmos. Chem. Phys., 10, 8551-8562, 2010.

Menon, S., Koch, D., Beig, G., Sahu, S., Fasullo, J., and Orlikowski, D.: Black carbon aerosols and the third polar ice cap, Atmos. Chem. Phys., 10, 4559-4571, 2010.

Ming, J., Zhang, D., Kang, S., and Tian, W.: Aerosol and fresh snow chemistry in the East Rongbuk Glacier on the northern slope of Mt. Qomolangma (Everest), J. Geophys. Res. -Atmos., 113, 10.1029/2008jd010430, 2008.

Ming, J., Xiao, C., Sun, J., Kang, S., and Bonasoni, P.: Carbonaceous particles in the atmosphere and precipitation of the Nam Co region, central Tibet, J. Environ. Sci., 22, 1748-1756, 2010.

Miyazaki, Y., Kawamura, K., and Sawano, M.: Size distributions and chemical characterization of water‐soluble organic aerosols over the western North Pacific in summer, J. Geophys. Res. -Atmos., 115, DOI: 10.1029/2010JD014439, 2010.

Psichoudaki, M., and Pandis, S. N.: Atmospheric Aerosol Water-Soluble Organic Carbon Measurement: A Theoretical Analysis, Environ. Sci. Technol., 47, 9791-9798, 2013.

Qian, Y., Flanner, M., Leung, L., and Wang, W.: Sensitivity studies on the impacts of Tibetan Plateau snowpack pollution on the Asian hydrological cycle and monsoon climate, Atmos. Chem. Phys., 11, 1929-1948, 2011.

Qian, Y., Yasunari, T. J., Doherty, S. J., Flanner, M. G., Lau, W. K., Ming, J., Wang, H., Wang, M., Warren, S. G., and Zhang, R.: Light-absorbing particles in snow and ice: Measurement and modeling of climatic and hydrological impact, Adv. Atmos. Sci., 32, 64-91, 2015.

Qiu, J.: The third pole, Nature, 454, 393-396, 2008.

Ram, K., Sarin, M. M., and Hegde, P.: Long-term record of aerosol optical properties and chemical composition from a high-altitude site (Manora Peak) in Central Himalaya, Atmos. Chem. Phys., 10, 11791-11803, 2010.

Ramanathan, V., Chung, C., Kim, D., Bettge, T., Buja, L., Kiehl, J. T., Washington, W. M., Fu, Q., Sikka, D. R., and Wild, M.: Atmospheric brown clouds: Impacts on South Asian climate and hydrological cycle, Proc. Natl. Acad. Sci. U. S. A., 102, 5326-5333, 2005.

Ramanathan, V., and Carmichael, G.: Global and regional climate changes due to black carbon, Nat.

569   Geosci., 1, 221-227, 2008.

570 Simoneit, B. R., Schauer, J. J., Nolte, C., Oros, D. R., Elias, V. O., Fraser, M., Rogge, W., and Cass, G. R.:
571   Levoglucosan, a tracer for cellulose in biomass burning and atmospheric particles, Atmos.
572   Environ., 33, 173-182, 1999.

573 Stocker, T. F., Dahe, Q., and Plattner, G.-K.: Climate Change 2013: The Physical Science Basis,
574   Working Group I Contribution to the Fifth Assessment Report of the Intergovernmental
575   Panel on Climate Change. Summary for Policymakers (IPCC, 2013), 2013.

576 Stone, E. A., Schauer, J. J., Pradhan, B. B., Dangol, P. M., Habib, G., Venkataraman, C., and
577   Ramanathan, V.: Characterization of emissions from South Asian biofuels and application
578   to source apportionment of carbonaceous aerosol in the Himalayas, J. Geophys. Res.
579   -Atmos., 115, doi:10.1029/2009JD011881, 2010.

580 Turpin, B. J., and Huntzicker, J. J.: Identification of secondary organic aerosol episodes and
581   quantitation of primary and secondary organic aerosol concentrations during SCAQS,
582   Atmos. Environ., 29, 3527-3544, 1995.

583 Vadrevu, K. P., Ellicott, E., Giglio, L., Badarinath, K. V. S., Vermote, E., Justice, C., and Lau, W. K. M.:
584   Vegetation fires in the himalayan region – Aerosol load, black carbon emissions and
585   smoke plume heights, Atmos. Environ., 47, 241-251, 2012.

586 Wan, X., Kang, S., Wang, Y., Xin, J., Liu, B., Guo, Y., Wen, T., Zhang, G., and Cong, Z.: Size distribution
587   of carbonaceous aerosols at a high-altitude site on the central Tibetan Plateau (Nam Co
588   Station, 4730ma. sl), Atmos. Res., 153, 155-164, 2015.

589 Wang, R., Tao, S., Balkanski, Y., Ciais, P., Boucher, O., Liu, J., Piao, S., Shen, H., Vuolo, M. R., and Valari,
590   M.: Exposure to ambient black carbon derived from a unique inventory and
591   high-resolution model, P. Natl. Acad. Sci. USA, 111, 2459-2463, 2014a.

592 Wang, X., Gong, P., Yao, T., and Jones, K. C.: Passive air sampling of organochlorine pesticides,
593   polychlorinated biphenyls, and polybrominated diphenyl ethers across the Tibetan
594   Plateau, Environ. Sci. Technol., 44, 2988-2993, 2010.

595 Wang, X., Xu, B., and Ming, J.: An overview of the studies on black carbon and mineral dust
596   deposition in snow and ice cores in East Asia, J. Meteorol. Res., 28, 354-370, 2014b.

597 Watson, J. G., Chow, J. C., and Houck, J. E.: PM2.5 chemical source profiles for vehicle exhaust,
598   vegetative burning, geological material, and coal burning in Northwestern Colorado
599   during 1995, Chemosphere, 43, 1141-1151, 2001.

600 Wu, G., and Zhang, Y.: Tibetan Plateau forcing and the timing of the monsoon onset over South
601   Asia and the South China Sea, Mon. Weather Rev., 126, 913-927, 1998.

602 Xia, X., Zong, X., Cong, Z., Chen, H., Kang, S., and Wang, P.: Baseline continental aerosol over the
603   central Tibetan plateau and a case study of aerosol transport from South Asia, Atmos.
604   Environ., 45, 7370-7378, 2011.

605 Xu, B., Cao, J., Hansen, J., Yao, T., Joswia, D. R., Wang, N., Wu, G., Wang, M., Zhao, H., Yang, W., Liu, X.,
606   and He, J.: Black soot and the survival of Tibetan glaciers, P. Natl. Acad. Sci. USA, 106,
607   22114-22118, 2009.

608 Xu, C., Ma, Y., Panday, A., Cong, Z., Yang, K., Zhu, Z., Wang, J., Amatya, P., and Zhao, L.: Similarities
609   and differences of aerosol optical properties between southern and northern sides of the
610   Himalayas, Atmos. Chem. Phys., 14, 3133-3149, 2014.

611 Yao, T., Thompson, L. G., Mosbrugger, V., Zhang, F., Ma, Y., Luo, T., Xu, B., Yang, X., Joswiak, D. R.,
612   Wang, W., Joswiak, M. E., Devkota, L. P., Tayal, S., Jilani, R., and Fayziev, R.: Third Pole

613   Environment (TPE), Environ. Dev., 3, 52-64, 2012.

614   Yasunari, T., Bonasoni, P., Laj, P., Fujita, K., Vuillermoz, E., Marinoni, A., Cristofanelli, P., Duchi, R.,
615   Tartari, G., and Lau, K. M.: Estimated impact of black carbon deposition during
616   pre-monsoon season from Nepal Climate Observatory-Pyramid data and snow albedo
617   changes over Himalayan glaciers, Atmos. Chem. Phys., 10, 6603-6615, 2010.

618   Zhao, Z., Cao, J., Shen, Z., Xu, B., Zhu, C., Chen, L. W. A., Su, X., Liu, S., Han, Y., and Wang, G.: Aerosol
619   particles at a high - altitude site on the Southeast Tibetan Plateau, China: Implications
620   for pollution transport from South Asia, J. Geophys. Res. -Atmos., 118, 11360-11375,
621   2013.

622   Zou, H., Zhou, L., Ma, S., Li, P., Wang, W., Li, A., Jia, J., and Gao, D.: Local wind system in the Rongbuk
623   Valley on the northern slope of Mt. Everest, Geophys. Res. Lett., 35, DOI:
624   10.1029/2008GL033466, 2008.

625

626

627

628

629 **Table 1**. Seasonal average abundances (along with standard deviation) of OC, EC, WSOC

630 and water soluble ionic species ($\mu g\ m^{-3}$), as well as the ratios of OC/EC and WSOC/OC.

	Annual	Pre-monsoon	Monsoon	Post-monsoon	Winter
Number	50	13	11	13	13
Carbonaceous components					
OC	1.43±1.16	2.61±1.58	0.81±0.14	1.06±0.53	1.14±0.50
EC	0.25±0.22	0.44±0.31	0.10±0.06	0.19±0.07	0.26±0.12
OC/EC	6.69±6.33	6.63±4.05	10.58±11.95	5.56±2.03	5.18±3.58
WSOC	0.77±0.60	1.28±0.87	0.49±0.25	0.71±0.26	0.54±0.29
WSOC/OC	0.58±0.24	0.47±0.09	0.59±0.28	0.62±0.23	0.57±0.27
Levoglucosan	0.019±0.037	0.047±0.064	0.004±0.003	0.007±0.005	0.014±0.008
Water-soluble inorganic ions					
Cl^-	0.02±0.03	0.04±0.04	0.01±0.01	0.02±0.02	0.02±0.04
NO_3^-	0.20±0.27	0.51±0.37	0.06±0.04	0.08±0.04	0.12±0.07
SO_4^{2-}	0.43±0.54	1.06±0.66	0.09±0.09	0.18±0.07	0.32±0.24
Na^+	0.07±0.06	0.13±0.06	0.04±0.04	0.04±0.03	0.06±0.05
NH_4^+	0.03±0.09	0.10±0.16	BDL	BDL	0.00±0.01
K^+	0.02±0.05	0.06±0.07	BDL	BDL	0.00±0.02
Ca^{2+}	0.88±0.56	1.19±0.48	0.50±0.18	1.01±0.75	0.79±0.36
Mg^{2+}	0.04±0.02	0.06±0.02	0.02±0.01	0.05±0.01	0.04±0.01

631 BDL, Below Detection Limits (0.01 $\mu g\ m^{-3}$ for cations and anions).

632

633

Table 2. Comparison of OC and EC concentrations (μg m^{-3}) and OC/EC ratios of aerosols from QOMS with other sites in the Himalayas and on the Tibetan

Plateau.

Location	Description	Sample	Sampling period	OC	EC	OC/EC	Method	Reference
QOMS	Southern TP(4276 m)	TSP	Aug 2009 - Jul 2010	1.43±1.16	0.25±0.22	6.7 (1.91-43.8)	TOR	This study
Nam Co	Central TP (4730 m)	TSP	Jul 2006-Jan 2007	1.66±0.79	0.082±0.07	31.9±31.1	TOR	(Ming et al., 2010)
Muztagh Ata,	Northwest TP(4500 m)	TSP	Dec 2003-Feb 2005	0.48	0.055	10 (2.9-32.1)	TOR	(Cao et al., 2009)
Qinghai Lake	Northeast TP (3200 m)	PM2.5	Jul-Aug 2010	1.58±0.59	0.37±0.24	5.9(1.85-21.8)	TOR	(Li et al., 2013)
Lulang	Southeast TP(3360 m)	TSP	Jul 2008-July 2009	4.28±2.05	0.52±0.35	1.7-58.4	TOR	(Zhao et al., 2013)
Tengchong	Southeast TP(1640 m)	PM10	Apr-May 2004	5.8±4.4	1.5±1.0	2.63	TOR	(Engling et al., 2011)
Manora Peak, India	Himalayas (1950 m)	TSP	Feb 2005-Jul 2008	8.2±5.2	1.3±1.2	7.3±3.4	TOT	(Ram et al., 2010)
NCO-P, Nepal	Himalayas(5079 m)	PM10	Premonsoon 2006-2008	2.4	0.5	4.8	TOT	(Decesari et al., 2010)
			Monsoon	0.9	0.1	9		
			Postmonsoon	1.4	0.1	14		
			Dry season	1.2	0.1	12		
Langtang, Nepal	Himalayas (3920 m)	PM2.5	Jun –Sep 1999	0.75±0.69	0.15±0.16	5.0	TOT	(Carrico et al., 2003)
			Oct 1999-Jan 2000	1.81±1.25	0.52±0.48	3.48		
			Feb-May 2000	3.44±4.19	0.48±0.38	7.17		
Godavari, Nepal	S. Himalayas (1600 m)	PM2.5	2006	4.8±4.4	1.0±0.8	4.8	TOT	(Stone et al., 2010)
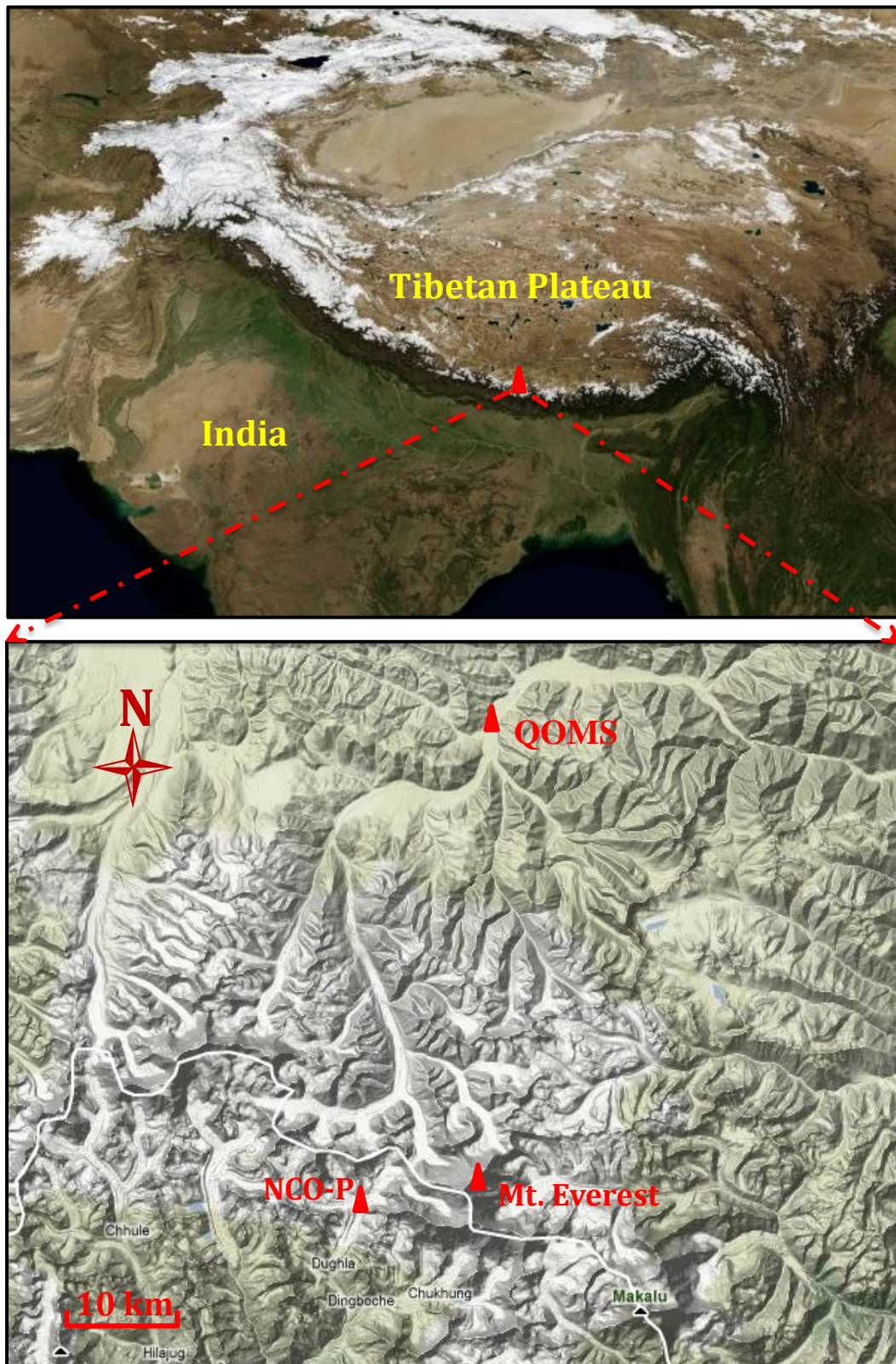
Fig. 1 Location of the sampling site (QOMS, 4276 m a.s.l.) at the south rim of the Tibetan Plateau, with the NCO-P (5079 m a.s.l.) and the summit of Mt. Everest (8844 m a.s.l.).
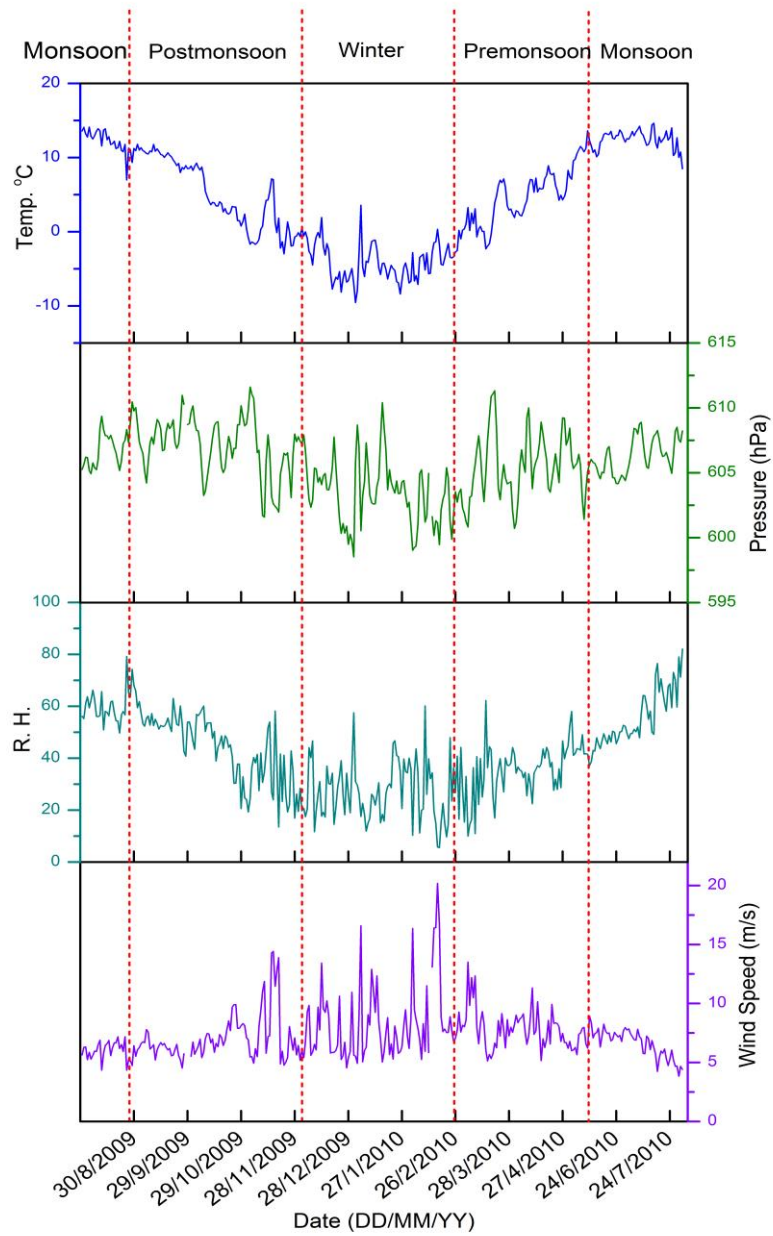
Fig. 2. Time-series of ambient temperature, atmospheric pressure, relative humidity and wind speed at QOMS from August 2009 to July 2010.
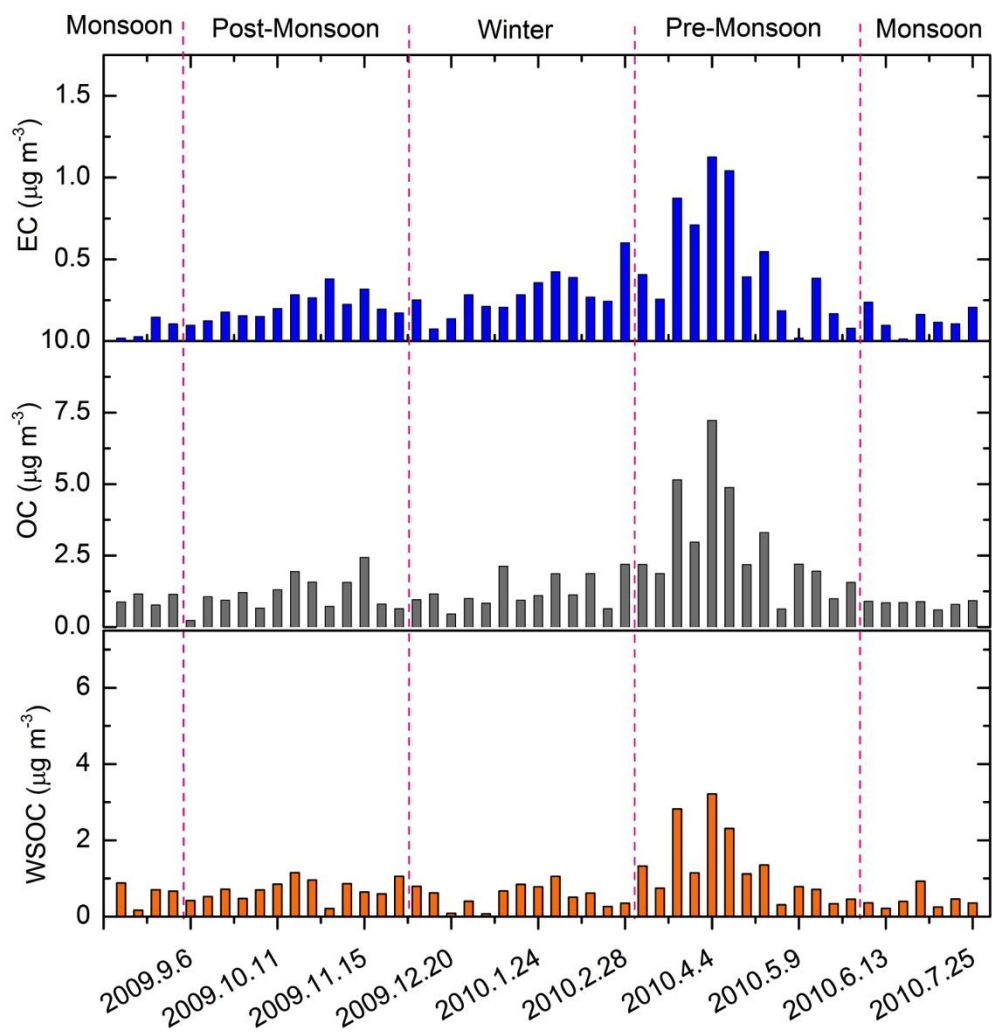
Fig. 3. Temporal variations (weekly) of OC, EC and WSOC at the QOMS site from August 2009 to July 2010.
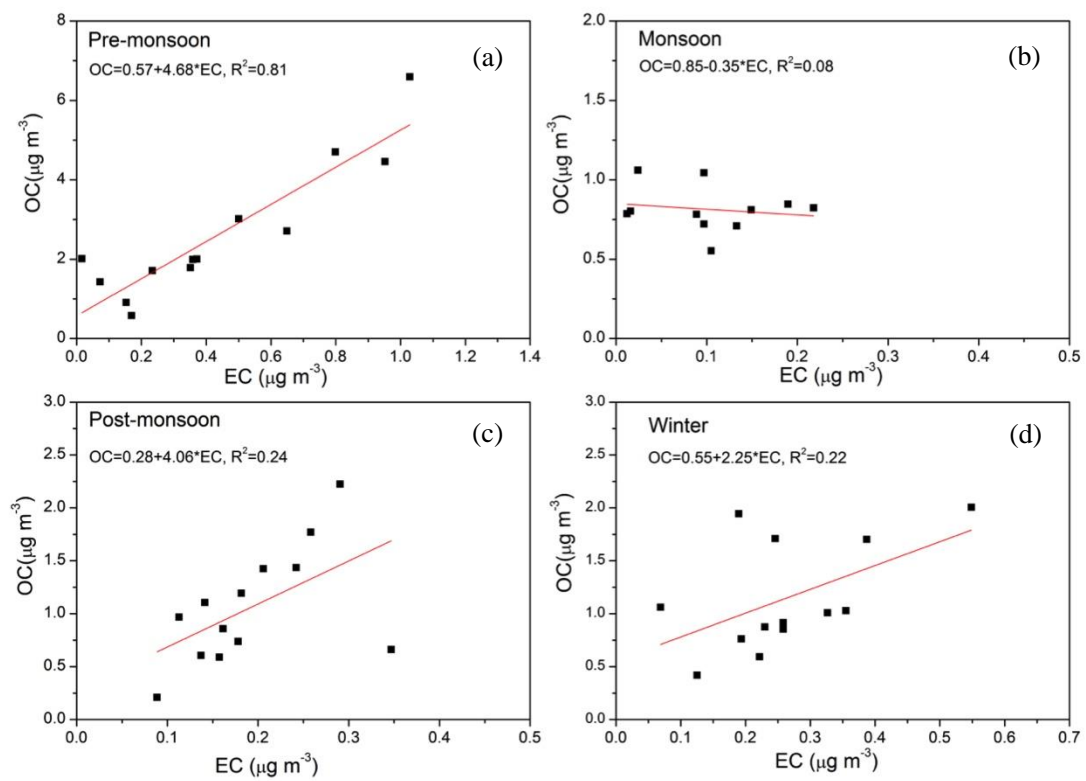
Fig. 4. Relationship between OC and EC in aerosols of different seasons at QOMS.
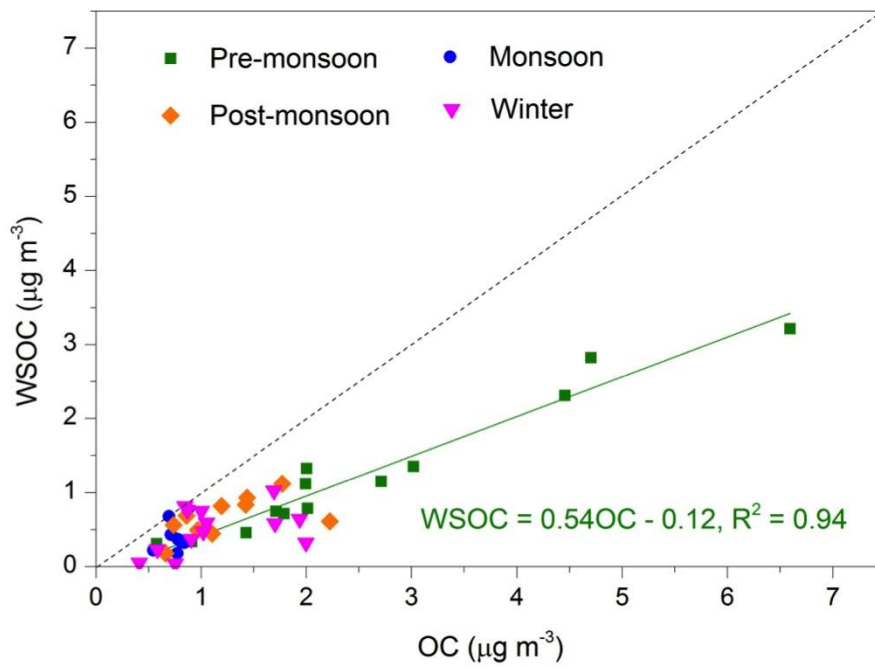
Fig. 5. Relationship between WSOC and OC in aerosols from QOMS.
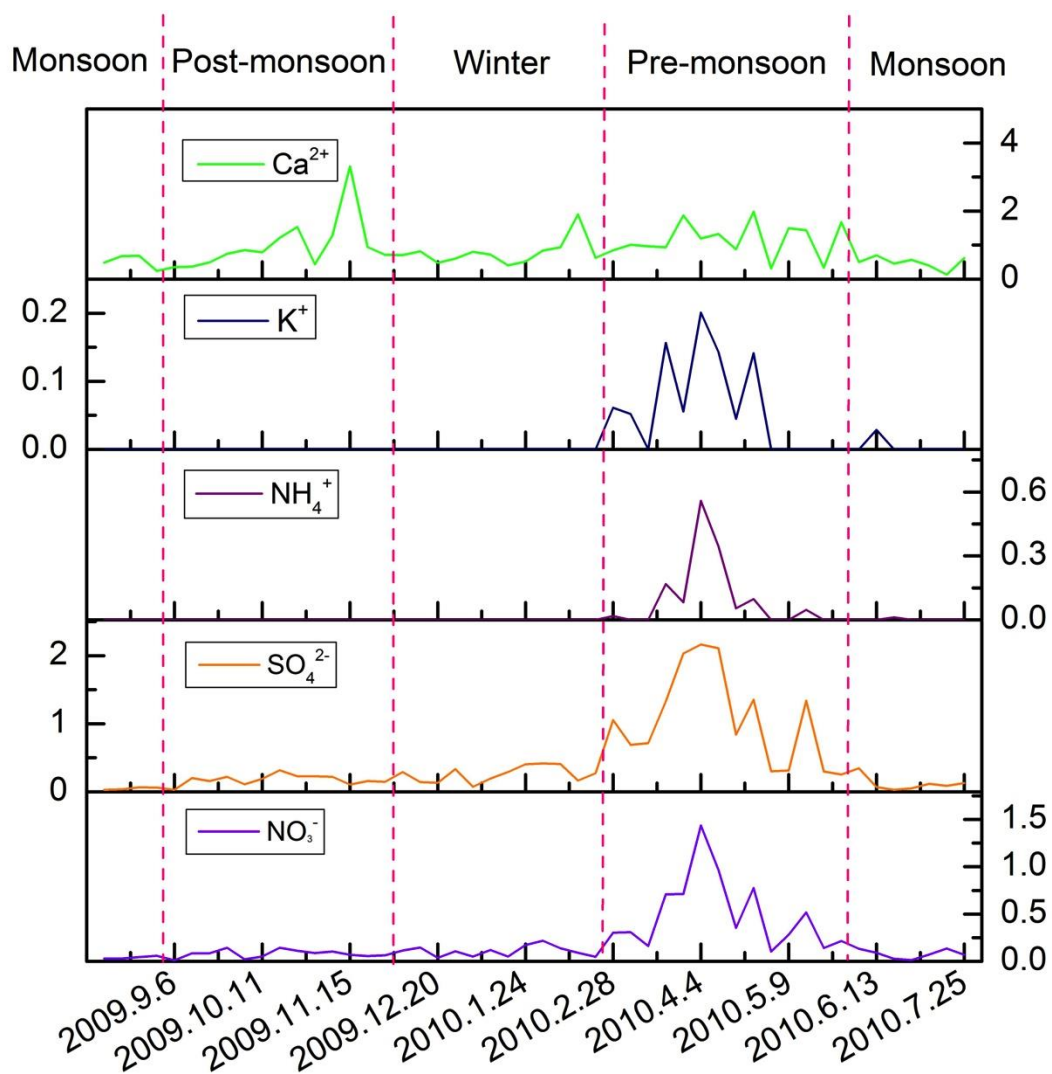
Fig. 6. Temperal variations (weekly) of water-soluble ionic species (Ca^{2+}, K^+, NH_4^+, SO_4^{2-} and NO_3^-) in aerosols collected at QOMS (Units: $\mu g\ m^{-3}$).
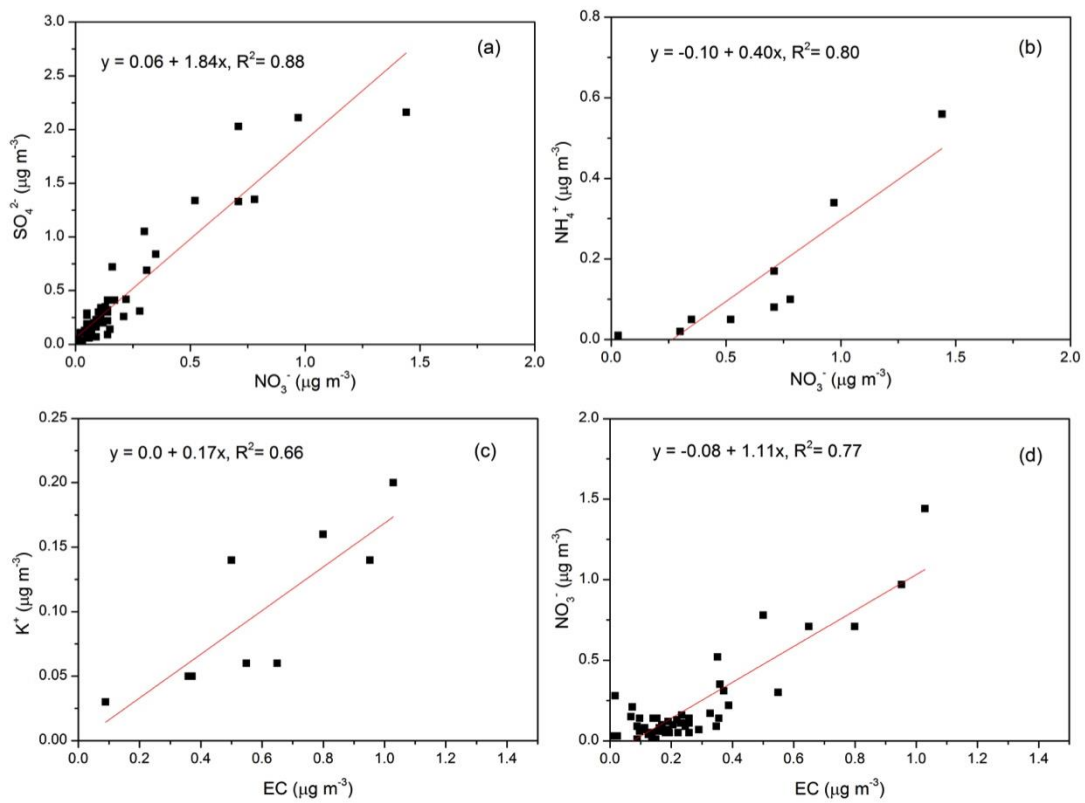
Fig. 7. Correlations between various chemical components. (a) SO_4^{2-} and NO_3^-, (b) NH_4^+ and NO_3^-, (c) K^+ and EC, (d) NO_3^- and EC.
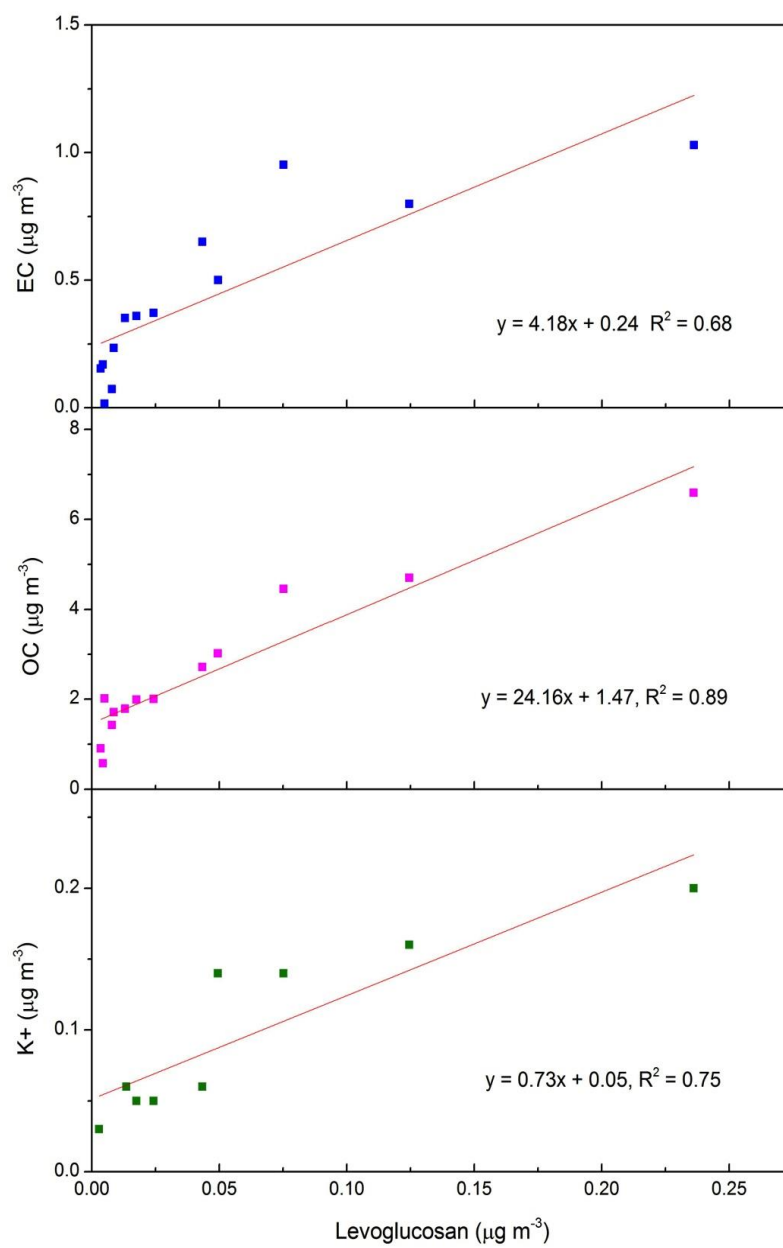
Fig. 8. The relationship between EC, OC, K$^+$ and levoglucosan in aerosols at QOMS during the pre-monsoon season, 2010.
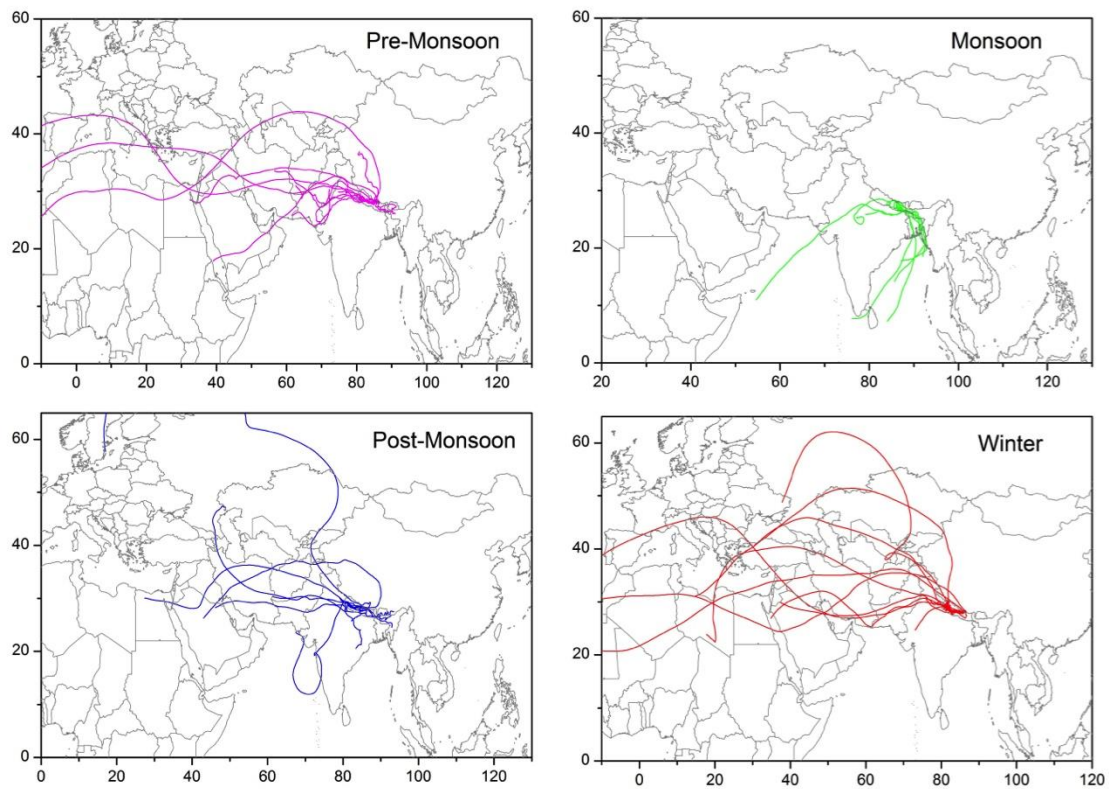
Fig. 9. Seven-day backward trajectories at QOMS on each sampling day during different seasons.
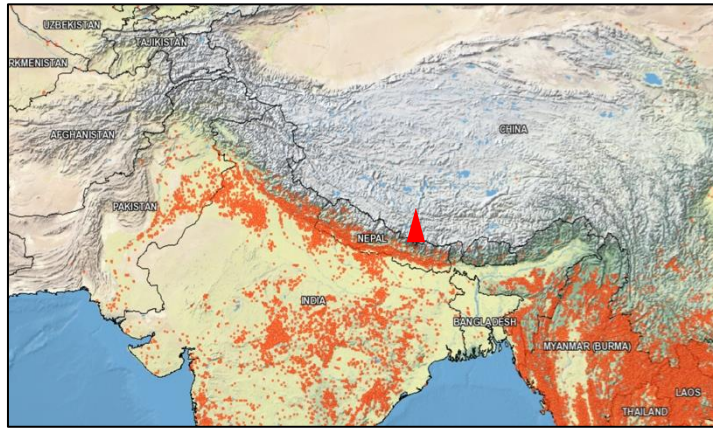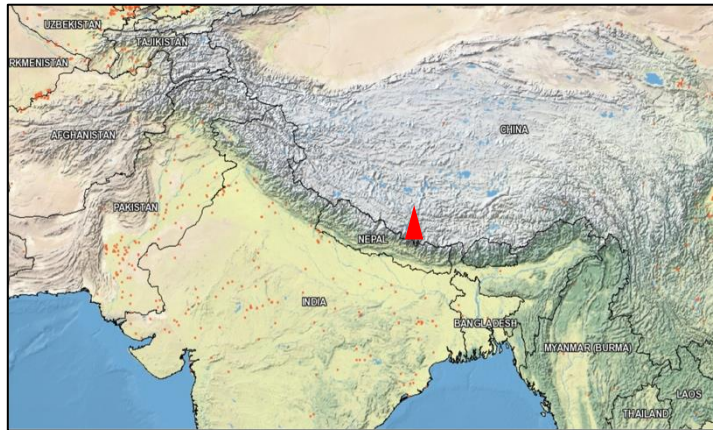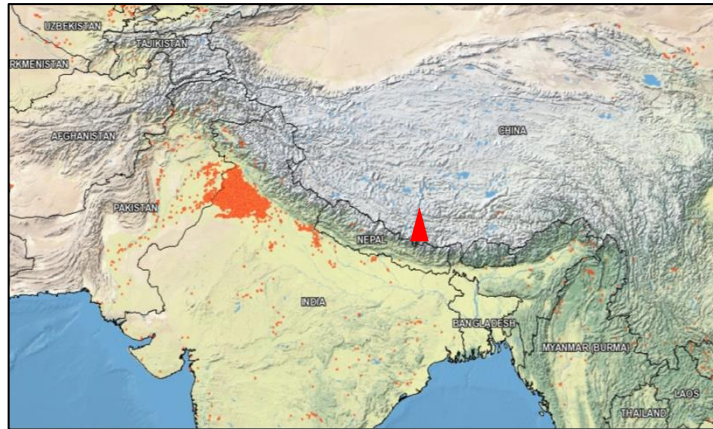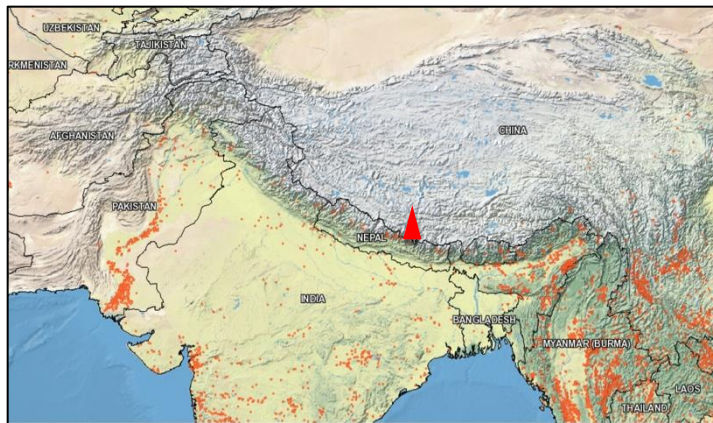
Fig. 10. The spatial distribution of fire spots observed by MODIS in different seasons (Aug. 2009 to Jul. 2010) (https://firms.modaps.eosdis.nasa.gov/firemap/).
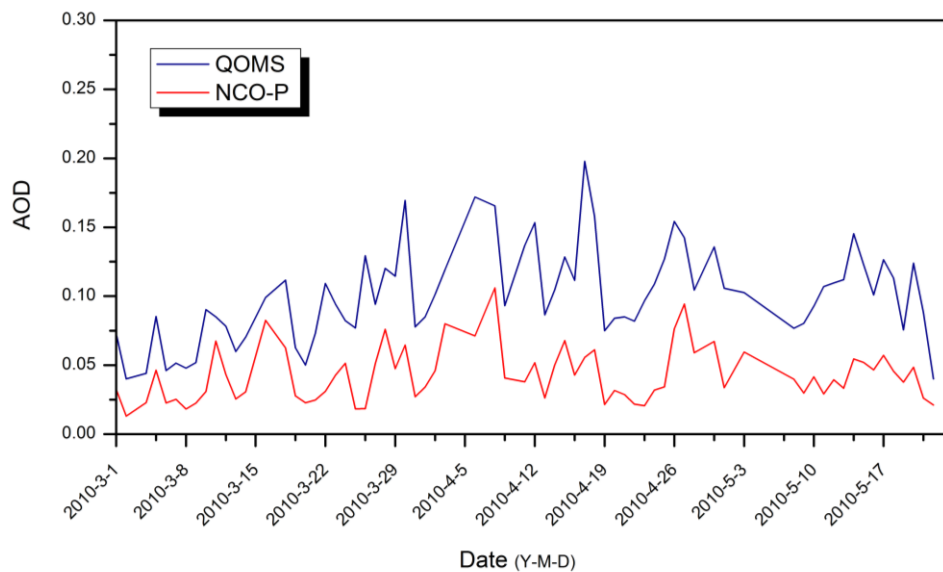
Fig. 11. The temporal variations of the daily aerosol optical depth (AOD, 500nm) at QOMS and NCO-P during the pre-monsoon season, 2010 (n=70).